



The force on a magneto-spherical particle oscillating in a viscous fluid perpendicular to an impermeable planar wall with slippage

Shreen El-Sapa

Department of Mathematics, Faculty of Science, Damanshour University, Damanshour, Egypt

Abstract. The effect of a magnetic field and slip on the motion of a solid sphere moving perpendicular to an unbounded rigid wall in an unlimited viscous fluid is investigated. As the sphere vibrates perpendicularly to the rigid wall, its center line is accompanied by a low amplitude vibration. A slip condition is applied to the sphere surface, while a no-slip dynamic condition is applied to the wall. Additionally, a semi-analytical method and a numerical scheme using collocation are presented. Furthermore, we calculate the amplitude of the non-dimensional coefficients of drag force acting on the solid sphere using various values of frequency, separation, and magnetic parameters. In addition, streamlines are plotted. The results of the magnitude normalized drag force are compared with those in previous literature.

2020 Mathematics Subject Classifications: 76-XX, 76DXX

Key Words and Phrases: Viscous Fluid, Magnetic Field, Oscillating Sphere, Slippage, Collocation Method

1. Introduction

Among the well-known fields in which the MHD field has a significant influence are magnetospheres, planetary celestials, chemical engineering, and electronic engineering, which play an important role in chemical, mechanical, biological, and medical fields. Cramer and Pai [1] studied the effects of a magnetic field upon a Stokes flow and their theory has been applied to a variety of geophysical, astrophysical, and engineering issues. According to Sellier and Aydin [2] axisymmetric magnetohydrodynamic movements can be produced in a conducting Newtonian flux region surrounded by a flat wall by classifying either radial or axial points forces on a circular ring established parallel with the wall and perpendicular to a uniform magnetic field. Corrugated curved channels are used for MHD flow [3]. Many researchers work about magnetic fields with normal convection in a permeable medium that has various implementations in energy, thermal geology, petrol extraction such as Qian and Bau [4] proved that MHD flows due to the oscillating plate.

DOI: <https://doi.org/10.29020/nybg.ejpam.v15i3.4442>

Email address: s_elsapa82@sci.dmu.edu.eg (S. El-Sapa)

Shreen and Noura [5] investigated the impacts of the magnetic field over two unequal rigid spheres of slip condition on the surfaces involved in a permeable medium under Stokes assumptions. In their analysis of magnetohydrodynamic flow over an unlimited vertical oscillating plate in a permeable medium, Chaudhary and Jain [6] analyzed the magneto-hydrodynamic flow over an unlimited vertical oscillating plate within a permeable medium, getting account of the appearance of mass transfer and free convection by using the Laplace-transform procedure. Also, Jawda et al. [7] applied MHD on Magneto-hydrodynamic flow of nanofluid in a channel with shape effects, Takhar et al. [8] studied MHD flow over a moving plate in a rotating fluid with magnetic field, Hall currents and free stream velocity. On the other side, Krishna et al. [9, 10] introduced hall and ion slip effects on unsteady MHD free convective rotating flow through a saturated porous medium over an exponential accelerated plate and hall and ion slip effects on MHD rotating flow of elasto-viscous fluid through porous medium. In addition, MHD has been applied to fluids flow in other ways, such as [11–15].

On the other hand, the oscillating flows have extensive interest in various chemical methods such as absorption, extraction, and engineering implementation, for example, floating movement of microorganisms and Brownian particle movement. Therefore, Chang-Yi Wang [16] studied the flow field induced by oscillating by using the method of inner and outer expansions experimentally. Rikitake [17] improved theories of magnetohydrodynamic oscillations of a conducting fluid sphere in a uniform magnetic field. Accordingly, Chawla [18] introduces the effect of harmonic oscillations in the magnitude of the free stream velocity on the magnetohydrodynamic boundary layer flow past a flat plate, in the presence of an aligned field. Also, many researchers have paid growing attention to the use of magnetic fluid for specific tasks related to magnetic-field-controlled vibration damping and modulation by oscillating in a magnetic fluid such as [19–23]. Moreover, Polunin et al. [24] expanded the physical understanding of the oscillating flow of magnetic fluid in the magnetic field by studying the effect in the thin near-wall layer under a strong transverse magnetic field. Therefore, Ryapolov et al. [25] described a study of the viscoelastic parameters of the system based on an element of magnetic fluid bounded by the surface of a horizontal plexiglass tube located in the field of an electromagnet that makes damped oscillation. Üstündağ et al. [26] used the keyhole during high-power laser beam welding in partial penetration mode by means of a high-speed camera where an oscillating magnetic field was applied perpendicular to the welding direction on the root site of the steel plate. Sherief et al. [27, 28] showed the problems of the rectilinear oscillations of two spherical particles along the line through their centers in an axisymmetric, viscous, incompressible flow at a low Reynolds number and wall interaction between a particle oscillates with the same frequency and with different amplitudes with no-slip and without magnetic field. Ashmawy [29] proposed the rotary oscillation of a composite sphere, consisting of a solid core surrounded by a porous shell, in an incompressible viscous fluid bounded by a concentric spherical cavity is investigated using the Brinkman model and applied stress jump condition.

Furthermore, the exploratory perception of slip occasions at frictional interfaces is testing and just a couple of effects of two-dimensional fronts have been accounted for up until now. Sweeney et al. [30] demonstrated to play a pivotal role in the distribution and magnitude of polycrystal slip relative to observed crack nucleation sites in the context of constrained cyclic microplasticity under effects of length scale. In addition, Basnayaka et al. [31] enhanced filtration rate has been modeled by superimposing a slip velocity at the boundary of the capillaries formed in the cake and evaluating the medium resistances by incorporating a slip into the filtration equation which varies with the concentration of hydrophobic reagent and the effective size of capillaries. Further, the numerical solutions are elucidated by using the collocation method, finite difference method, and Runge-Kutta based shooting technique. Furthermore, Sulochana et al. [32] presented the study as a numerical investigation of the flow, heat, and mass transfer behavior of magnetohydrodynamic flow over a vertical rotating cone through a porous medium in the presence of thermal radiation, chemical reaction, and Soret effects by using Runge-Kutta based shooting technique. Therefore, Veera Krishna et al. [33] investigated the effects of thermal radiation and rotation on the unsteady MHD convective flow past an infinite vertical moving absorbent plate and employed to migrate the governing partial differential equations in a system of non-linear ordinary differential equations and elucidated computationally by making use of cubic B-splines collocation method. Many researchers used a collocation method such as [34–39].

The purpose of this study was to investigate the impact of slip effects and magnetic fields on the interaction between an oscillating sphere in a viscous fluid moving towards a rigid wall. The sphere oscillates rectilinearly normal to an impermeable bounding plane wall. Numerical solutions of the amplitude drag force were obtained by using a collocation method. Besides, the influence of non-dimensional governing parameters on normalized drag force with different slip, separation, frequency, and magnetic parameters are determined and discussed with the help of graphs and tables.

2. Field Equations

Under the Stokesian approximation, the field equations governing an incompressible unsteady viscous fluid flow under a uniform magnetic field are given in vector forms as:

(i) Conservation of mass

$$\nabla \cdot \vec{u} = 0, \quad (1)$$

(ii) Conservation of momentum

$$\rho \frac{\partial \vec{u}}{\partial t} = \mu \nabla^2 \vec{u} - \nabla p + \frac{1}{c} \vec{J} \wedge \vec{B}. \quad (2)$$

where \vec{u} is the volume averaged velocity parallel to the wall, p is the pore average pressure, μ represents the kinematic viscosity, ρ is the density of the fluid, and c is the speed of

light . Also, $\vec{J} = \frac{\sigma_0}{c} \vec{u} \wedge \vec{B}$, $\wedge \vec{B} = \mu_0 \wedge \vec{H}$, where \vec{J} , \vec{B} and \vec{H} are the current density, the magnetic induction, the magnetic field respectively, σ_0 is the electrical conductivity and μ_0 is the magnetic permeability. The constitutive equations for the stress tensor Π can be written as:

$$\Pi = -pI + 2\mu\Delta, \quad (3)$$

where $\Delta = \frac{1}{2} (\nabla\vec{u} + \nabla^T\vec{u})$ is the deformation tensor, and I is the unit dyadic. Here $(.)^T$ denotes for transpose.

2.1. General Slip-Boundary Conditions

At a surface of the sphere, we shall assume slip and use the most likely hypothesis [5, 15], In our case this hypothesis takes the form:

$$(\vec{u} - U\vec{e}_z) = \beta(I - \vec{n}\vec{n}) \cdot (\vec{n} \cdot \Pi) \quad (4)$$

where

- (i) This coefficient β , is a measure of the degree of tangential slip existing between the fluid and the solid at its surface.
- (ii) It is assumed to depend only on the nature of the fluid and solid surface.
- (iii) In the limiting case of $\beta \rightarrow \infty$, there is a perfect slip at the particle surface and the particle acts like a spherical gas bubble, while the standard no-slip boundary condition for solids is obtained by letting $\beta \rightarrow 0$.
- (iv) Experimentally, the slip has been measured for liquids under various physical and geometrical circumferences. Therefore, some authors have used a different parameterization for the slip e.g. (Happel and Brenner 1983, Saad 2012, Lee and Keh 2013, Faltas and Shreen 2019).

3. Mathematical Formulation

Consider a solid spherical particle that is oscillating and traveling axisymmetrically while immersed in an unbounded magnetic viscous fluid. The distance of the sphere center to the wall is b . In order to conveniently describe the surfaces of the sphere and plane, we choose the sphere center as the origin and use both the spherical polar coordinates system (r, θ, ϕ) and the cylindrical coordinates (ρ, ϕ, z) , The relations between the two coordinate systems are:

$$r^2 = \rho^2 + z^2, \quad \theta = \cos^{-1} \left(\frac{z}{r} \right) \quad (5)$$

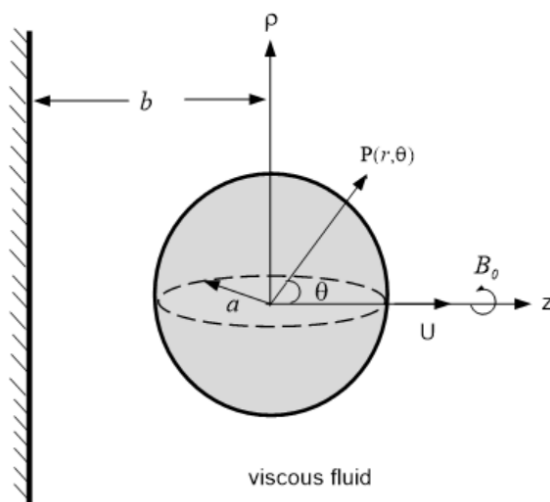


Figure 1: Diagram of a magnetic sphere oscillating perpendicular to a plane wall.

The flow generated is axially symmetric and all the flow functions are independent of ϕ . We can choose the velocity vector, the pressure, and the stream function as:

$$\vec{u} = u(r, \theta) e^{i\vartheta t}, \quad p = p(r, \theta) e^{i\vartheta t}, \quad \Psi = \Psi(r, \theta) e^{i\vartheta t}, \tag{6}$$

where ϑ , is the frequency of oscillation. Using equation (1), we write the velocity components in terms of the stream function Ψ in the cylindrical coordinates as:

$$u_\rho = -\frac{1}{\rho} \frac{\partial \Psi}{\partial z}, \quad u_z = \frac{1}{\rho} \frac{\partial \Psi}{\partial \rho}. \tag{7}$$

Introducing the non – dimensional quantities and assume that ϑ^{-1} is the typical time:

$$r^* = \frac{r}{a}, \rho^* = \frac{\rho}{a}, z^* = \frac{z}{a}, \tau^* = \tau a, \zeta^* = \zeta a, \Psi^* = \frac{\Psi}{U a^2}, \Pi^* = \frac{a \Pi}{\mu U}, P^* = \frac{a p}{\mu a}. \tag{8}$$

We normalize all lengths with respect to the characteristic radius of the sphere, a and since the velocity of fluid is not perpendicular to magnetic induction vector, we will use Lorentz’s average force over all directions of magnetic induction, keeping the symmetry of the flow, $\vec{B} = B_0 \vec{e}_\phi$, B_0 is a constant used by (Yadav [40] and El-Sapa [39]). Substituting from equation (8) into equation (2) we get:

$$R_e S_t \frac{\partial \vec{u}}{\partial t} = \nabla^2 \vec{u} - \nabla p - \frac{a^2 \sigma_0 B_0^2}{\mu c^2} \vec{u}, \tag{9}$$

where

- $R_e = \frac{U a}{\nu}$ is the magnetic Reynolds number.
- a is a characteristic length.

- $S_t = \frac{\vartheta a}{U}$ is the Strouhal number.
- B_0 is the magnetic induction.

Physically, R_e must be small and the Strouhal number, S_t must be large or $\frac{U}{\vartheta a} \ll 1$ implies that the amplitude of the oscillation is small compared with a . Since the speed $U\vec{e}_z$ is supposed to be small, therefore the assumption of the Stokesian flow may be used (a) The magnetic Reynolds number is small, so that the induced magnetic field is negligible in comparison with the imposed magnetic field and (b) The electric field is zero, because no applied or polarization voltages exist (Mayer, 1958).

The problem is then governed by the following equations:

$$\frac{\partial p}{\partial r} - \frac{k^2}{r^2 \sin \theta} \frac{\partial \Psi}{\partial \theta} + \frac{1}{r^2 \sin \theta} \frac{\partial}{\partial \theta} (E^2 \Psi) = 0, \quad (10)$$

$$\frac{1}{r} \frac{\partial p}{\partial \theta} + \frac{k^2}{r \sin \theta} \frac{\partial \Psi}{\partial r} - \frac{1}{r \sin \theta} \frac{\partial}{\partial r} (E^2 \Psi) = 0, \quad (11)$$

Elimination the pressure from equations (10) and (11) gives a fourth-order linear partial differential equation satisfied by the stream function:

$$E^2(E^2 - k^2)\Psi = 0, \quad (12)$$

where $k = \sqrt{i\chi^2 + \alpha^2}$, $\chi = \sqrt{\frac{\vartheta^2 a^2}{\nu}}$, $\alpha = \sqrt{\frac{a^2 \sigma_0 B_0^2}{\mu c^2}}$ are the frequency parameter and the magnetic parameter while the Stokesian operator is: $E^2 = \frac{\partial^2}{\partial r^2} + \frac{1-\xi^2}{r^2} \frac{\partial^2}{\partial \xi^2}$ and $\xi = \cos \theta$.

3.1. Boundary Conditions to the Problem

- (i) The boundary condition of relative normal velocity at $r = a$:

$$u_\rho = \beta t_{r\theta} \cos \theta, \quad (13)$$

- (ii) The dynamical boundary condition at $r = a$ (Basset, 1961 Happel and Brenner, 1983, Sherief et al., 2019):

$$u_z = U - \beta t_{r\theta} \sin \theta, \quad (14)$$

- (iii) The no-slip boundary conditions along the wall $z = b$ are given by:

$$u_\rho = 0, \quad u_z = 0, \quad (15)$$

- (iv) Moreover, at large distances from the spherical particles $r \rightarrow \infty$, the velocity components tend to zero, that is:

$$u_\rho \rightarrow 0, \quad u_z \rightarrow 0 = 0, \quad (16)$$

4. Method of solution

The solution of equation (12) can be expressed in the form:

$$\Psi = \Psi_s + \Psi_w, \quad (17)$$

where

$$E^2\Psi_s = 0, \quad E^2(E^2 - k^2)\Psi_w = 0, \quad (18)$$

where the part Ψ_s represents the general solution of the Stokes equation in the spherical coordinates. It can be expressed as an infinite series containing all the simply separable solutions in spherical coordinates which give a vanishing fluid velocity as $r \rightarrow \infty$ by Happel and Brenner [41] and the regular solution of part Ψ_s from equation (18) is given as:

$$\Psi_s(r, \theta) = \sum_{n=2}^{\infty} \left(A_n r^{-n+1} + B_n r^{\frac{1}{2}} K_{n-\frac{1}{2}}(kr) \right) \mathfrak{S}_n(\xi), \quad (19)$$

where A_n and B_n are the unknown constants which will be determined using the boundary conditions and $\mathfrak{S}_n(\cdot)$ is the Gegenbauer function of the first kind of order n and degree $(-\frac{1}{2})$ and $K_n(\cdot)$ is the modified Bessel function of the second kind of order n . The part Ψ_w from equation (18) represents the regular solution of the Stokes equation in the cylindrical coordinates is given by the Fourier-Bessel integral as:

$$\Psi_w(\rho, z) = \int_0^{\infty} \left(A(\tau) e^{-\tau z} + B(\tau) e^{-\xi z} \right) \rho J_1(\rho\tau) d\tau, \quad (20)$$

where $A(\tau)$ and $B(\tau)$ are unknown functions of the separation variable τ and $J_1(\rho\tau)$ is the Bessel function of the first kind of order unity. The general solution is:

$$\begin{aligned} \Psi &= \sum_{n=2}^{\infty} \left(A_n r^{-n+1} + B_n r^{\frac{1}{2}} K_{n-\frac{1}{2}}(kr) \right) \mathfrak{S}_n(\xi) \\ &+ \int_0^{\infty} \left(A(\tau) e^{-\tau z} + B(\tau) e^{-\xi z} \right) \rho J_1(\rho\tau) d\tau, \end{aligned} \quad (21)$$

where $\xi = \sqrt{\tau^2 + k^2}$. By using the equations (7) and (21) with the properties of Gegenbauer and Legendre functions and the chain rule we get the radial, axial velocity components and stress of the flow field in cylindrical coordinates are obtained:

$$a^2 u_\rho = \sum_{n=2}^{\infty} (A_n A_{1n}(\rho, z) + B_n B_{1n}(\rho, z)) \mathfrak{S}_n(\xi) + \int_0^{\infty} \tau L(\tau, z) J_1(\rho\tau) d\tau, \quad (22)$$

$$a^2 u_z = \sum_{n=2}^{\infty} (A_n A_{2n}(\rho, z) + B_n B_{2n}(\rho, z)) \mathfrak{S}_n(\xi) + \int_0^{\infty} \tau M(\tau, z) J_1(\rho\tau) d\tau, \quad (23)$$

$$\frac{at_r\theta}{\mu} = \sum_{n=2}^{\infty} (A_n A_{3n}(\rho, z) + B_n B_{3n}(\rho, z)) \mathfrak{S}_n(\xi)$$

$$+ \int_0^{\infty} \tau (R(\rho, z) J_1(\rho\tau) + S(\rho, z) J_0(\rho\tau)) d\tau, \quad (24)$$

where the definitions of the functions $A_{1n}, B_{1n}, A_{2n}, B_{2n}, A_{3n}, B_{3n}$ and also $R(\rho, z)$ and $S(\rho, z)$ are listed in Appendix A. Moreover, we obtained two linear algebraic equations which can be solved simultaneously to give the unknown functions $A(\tau)$ and $B(\tau)$ as follows:

$$A(\tau) = -e^{-\tau b} (\tau - \xi)^{-1} (\tau L(\tau, -b) - \xi M(\tau, -b)), \quad (25)$$

$$B(\tau) = -\tau e^{-\tau b} (\tau - \xi)^{-1} (M(\tau, -b) - L(\tau, -b)), \quad (26)$$

Applying the boundary conditions from equations (15) and (16) on the wall $z = -b$:

$$\left. \begin{aligned} \int_0^{\infty} \tau L(\tau, -b) J_1(\rho\tau) d\tau &= - \sum_{n=2}^{\infty} (A_n A_{1n} + B_n B_{1n}), \\ \int_0^{\infty} \tau M(\tau, -b) J_1(\rho\tau) d\tau &= - \sum_{n=2}^{\infty} (A_n A_{2n} + B_n B_{2n}). \end{aligned} \right\} \quad (27)$$

The expressions (27) can be easily inverted and integration can be performed using results of Hankel transforms:

$$L(\tau, -b) = - \int_0^{\infty} t \sum_{n=2}^{\infty} (A_n A_{1n} + B_n B_{1n}) J_1(t\tau) dt, \quad (28)$$

$$M(\tau, -b) = - \int_0^{\infty} t \sum_{n=2}^{\infty} (A_n A_{2n} + B_n B_{2n}) J_1(t\tau) dt. \quad (29)$$

The expressions can be now rewritten as:

$$A(\tau) = -e^{-\tau b} (\tau - \xi)^{-1} \sum_{n=2}^{\infty} \left[(\tau e_{1n}(\tau, -b) - \xi e_{2n}(\tau, -b)) A_n + (\tau f_{1n}(\tau, -b) - \xi f_{2n}(\tau, -b)) B_n \right], \quad (30)$$

$$B(\tau) = \tau e^{-\xi b} (\tau - \xi)^{-1} \sum_{n=2}^{\infty} \left[(e_{1n}(\tau, -b) - e_{2n}(\tau, -b)) A_n + (f_{1n}(\tau, -b) - f_{2n}(\tau, -b)) B_n \right]. \quad (31)$$

The integrals required in equations (30) and (31) are performed analytically as follows, Using the polynomial representations of the Gegenbauer and Legendre functions together with the result given by Erdelyi et al. [42]:

$$\int_0^{\infty} \frac{x^{\nu+\frac{1}{2}}}{(x^2 + a^2)^{\mu+1}} J_{\nu}(xy) (xy)^{\frac{1}{2}} dx = \frac{a^{\nu-\mu} y^{\mu+\frac{1}{2}}}{2^{\mu} \Gamma(\mu+1)} K_{\nu-\mu}(ay),$$

$$\Re\{a\} > 0, y > 0, -1 < \Re\{\nu\} < 2\Re\{\mu\} + 1 \tag{32}$$

$$\int_0^\infty \frac{x^{\nu+\frac{1}{2}} K_\mu(a(x^2 + y^2)^{\frac{1}{2}})}{(x^2 + \beta^2)^{\frac{\mu}{2}}} J_\nu(xy)(xy)^{\frac{1}{2}} dx = \frac{\beta^{\nu-\mu+1} y^{\mu+\frac{1}{2}}}{a^\mu} (y^2 + a^2)^{\mu-\nu-1} \times K_{\mu-\nu-1}(\beta(y^2 + a^2)^{\frac{1}{2}}), \Re\{a\} > 0, \Re\{\beta\} > 0, \tag{33}$$

where K_ν , is the modified Bessel function of the second kind, one can show by induction that:

$$\int_0^\infty \frac{1}{(t^2 + b^2)^{\frac{n}{2}}} \mathfrak{S}_{n+1}\left(\frac{-b}{(t^2 + b^2)^{\frac{1}{2}}}\right) J_1(t\tau) dt = \frac{(-1)^{n-1} \tau^{n-1}}{(n+1)!} e^{-\alpha b} \tag{34}$$

$$\begin{aligned} \int_0^\infty (t^2 + b^2)^{\frac{-1}{4}} \left(-\alpha b K_{n-\frac{3}{2}}(\alpha\sqrt{\rho^2 + b^2}) \mathfrak{S}_n(-b/\sqrt{\rho^2 + b^2}) \times \right. \\ \left. + (n+1) K_{n-\frac{1}{2}}(\alpha\sqrt{\rho^2 + b^2}) \mathfrak{S}_{n+1}(-b/\sqrt{\rho^2 + b^2}) \right) J_1(t\tau) dt \\ = (-1)^n \sqrt{\frac{\pi\alpha}{2\tau^2}} e^{-b\xi} \mathfrak{S}_n\left(\frac{\xi}{\alpha}\right) \end{aligned} \tag{35}$$

$$\int_0^\infty \frac{t}{(t^2 + b^2)^{-\frac{n+1}{2}}} P_n\left(\frac{-b}{(t^2 + b^2)^{\frac{1}{2}}}\right) J_0(t\tau) dt = \frac{(-1)^n \tau^{n-1}}{(n)!} e^{-\tau b} \tag{36}$$

$$\begin{aligned} \int_0^\infty t(t^2 + b^2)^{\frac{-3}{4}} \left(-\alpha\sqrt{t^2 + b^2} K_{n-\frac{3}{2}}(\alpha\sqrt{t^2 + b^2}) \mathfrak{S}_n(-b/\sqrt{t^2 + b^2}) \times \right. \\ \left. + K_{n-\frac{1}{2}}(\alpha\sqrt{t^2 + b^2}) P_n(-b/\sqrt{t^2 + b^2}) \right) J_0(t\tau) dt \\ = (-1)^{n-1} \sqrt{\frac{\pi\alpha}{2\xi^2}} e^{-b\xi} \mathfrak{S}_n\left(\frac{\xi}{\alpha}\right) \end{aligned} \tag{37}$$

To determine the unknown A_n, B_n we apply the boundary conditions on the sphere $r = a$:

$$\sum_2^\infty \left\{ A_n \left(\gamma_{1n}^{(1)}(1, \theta) - \beta \cos \theta \gamma_{1n}^*(1, \theta) \right) + B_n \left(\gamma_{2n}^{(1)}(1, \theta) - \beta \cos \theta \gamma_{2n}^*(1, \theta) \right) \right\} = 0, \tag{38}$$

$$\sum_2^\infty \left\{ A_n \left(\gamma_{1n}^{(2)}(1, \theta) - \beta \sin \theta \gamma_{1n}^*(1, \theta) \right) + B_n \left(\gamma_{2n}^{(2)}(1, \theta) - \beta \sin \theta \gamma_{2n}^*(1, \theta) \right) \right\} = U. \tag{39}$$

Accordingly, following the procedure developed by Chadwick, Z. Liao [43], Happel and Brenner [41] or by Sherief et al [39] or by Shreen and Faltas [28], the force exerted by the

micropolar fluid on the body in the positive z - direction, in the presence of a transverse magnetic field [44] and [45], is given by:

$$F_z = \pi\mu \int_C \rho^3 \frac{\partial}{\partial n} \left[\frac{E^2 \Psi}{\rho^2} - \frac{ik}{\nu} \rho \Psi \right] ds, \quad (40)$$

where ds is an arc length of a meridian curve C on the surface of the body. If the medium is unbounded, we may obtain a simpler formula for the drag force. Following a procedure similar that used by Lawrence and Weinbaum [45], we obtain F_z in the form

$$F_z = k^2 \left[V + 4\pi \lim_{r \rightarrow \infty} \frac{r^3 \Psi}{\rho^2} \right], \quad (41)$$

where V is the volume of the body and $\rho = r \sin \theta$. Formula (41) is applied under the condition of no fluid motion at infinity. Aside from the restriction to axisymmetric flow, no assumption is made about the shape of the body, see Fig.1. The result may then be used for flows involving porous bodies, droplets, non spherical bodies, interactions among bodies and interact between bodies and surfaces. This formula is applied also regardless of the boundary conditions satisfied at the surface of the body. Note that this formula is singular as $k \rightarrow 0$ by [46] and does not reduce to the corresponding formula in the absence of the transverse magnetic field.

Therefore, (41) reduces to:

$$F_z = 2\pi\mu k^2 \left(\frac{2}{3} a^3 U - 2A_2 \right) e^{-i\theta t} \quad (42)$$

where the hydrodynamic drag force F_∞ over an oscillating solid sphere a moves through unbounded viscous fluid in the absent of the plane wall with no-slip surface. It is given by Happel and Brenner [41]:

$$F_\infty = -6\pi\mu U a \left(1 + k + \frac{1}{9} k^2 \right) e^{-i\theta t} \quad (43)$$

From equations (41) and (42), the normalized drag, F can be put in the form:

$$\frac{F_z}{F_\infty} = K + iK', \quad (44)$$

where the magnitude normalized drag force and the phase angle are obtained as:

$$\left| \frac{F_z}{F_\infty} \right| = \sqrt{K^2 + K'^2}, \quad \Theta = \tan^{-1} \left(\frac{K'}{K} \right) \quad (45)$$

where K and K' are real force coefficients. Physically, they are the in phase and out-of-phase force oscillations, respectively and the phase angle is Θ .

5. Results and Numerical Discussions

The proposed semi-analytical method (collocation method) scheme can be used for solving the problem. Interactions between the sphere and the rigid wall under the uniform magnetic field are obtained. The results for the magnitude of the normalized drag are presented in Figs. 2-10 and Table 1 for different parameters, frequency, χ separation, $\lambda = b/a$ magnetic, α and the slip on the sphere, $\eta = \frac{\mu}{a}\beta$. The results converge to at least the significant figures shown in the table and the number of collocation points needed, $N = 60$ for each case listed in the table. Consequently, there are two (high-frequency and low-frequency) oscillation regimes that attenuate with constant time. An important benefit of fluctuations between values of the frequency and magnetic field is damping torsional oscillation. As expected, the plots show that as $\lambda \rightarrow 0$ (i.e., increasing gap thickness between the sphere and the plate), $|F/F_\infty| \rightarrow 1$ where a further increase in amplitude caused the spheres to detach from each other and oscillate separately. Furthermore, Fig.2 shows that the magnitude of drag force decreases with increases of both the separation parameter for values $\lambda = 0.001, 0.1, 0.25, 0.5$ and the corresponding magnetic parameter $\alpha = 1, 10$ at a certain value of the frequency $\lambda = 1$ and also decreases with monotonically increases of the slip to be stable after $\eta = 2$ for perfect slip. As the liquid amplitude was increased under conditions of constant frequency, lateral oscillation of the sphere began to occur.

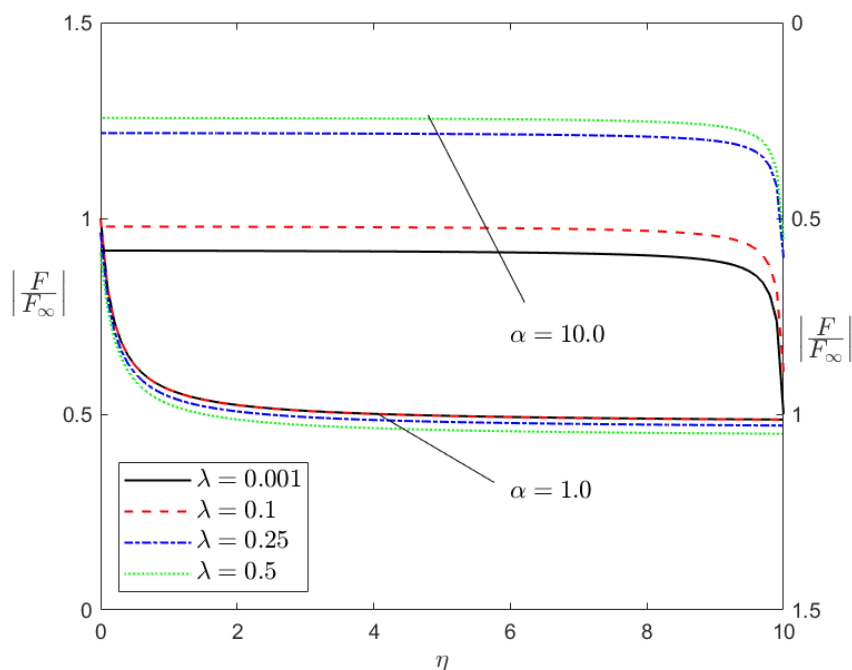


Figure 2: Magnitude normalized drag force versus slip at different magnetic and separation parameters with frequency $\chi = 1.0$.

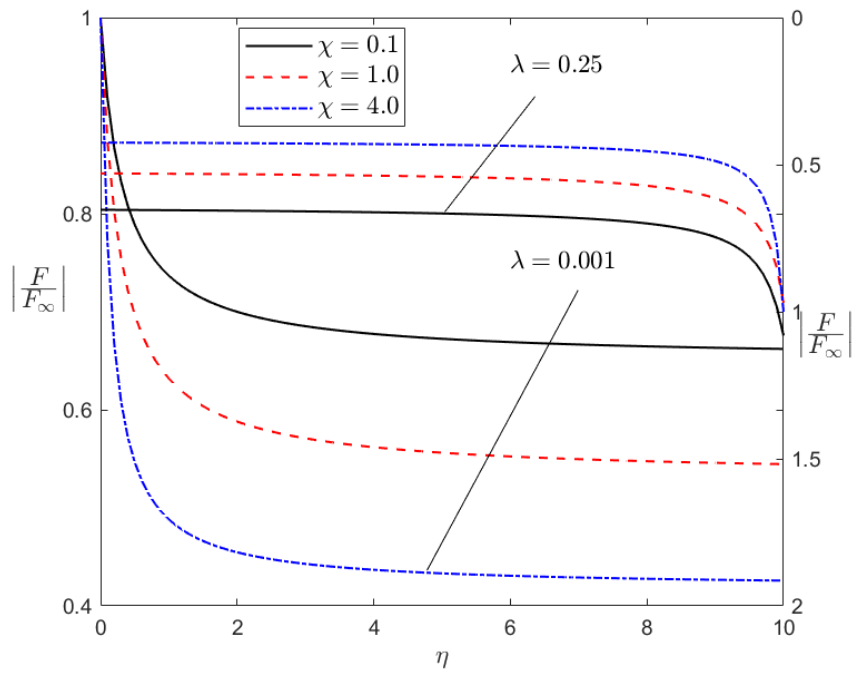


Figure 3: Magnitude normalized drag force versus slip at different frequency and separation parameters with magnetic parameter $\alpha = 0.01$.

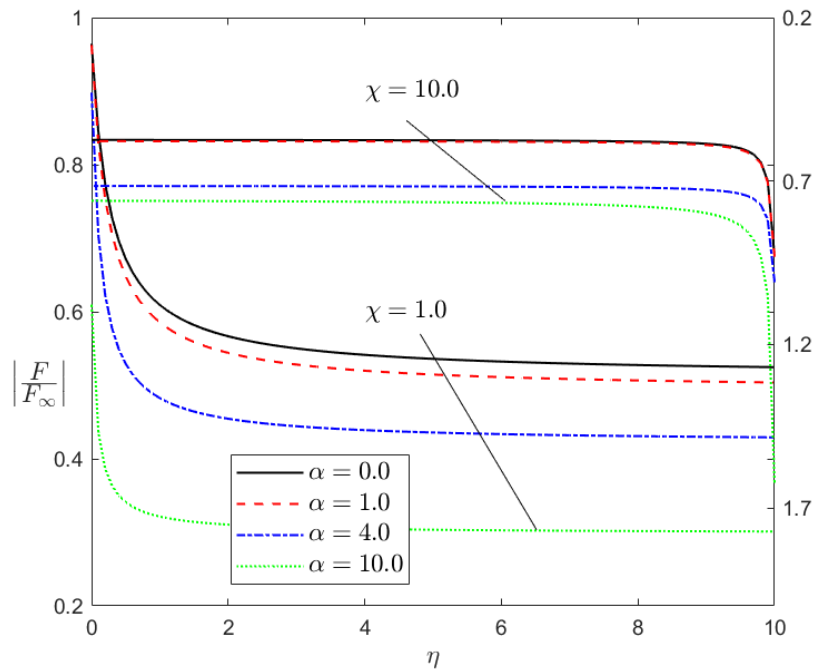


Figure 4: Magnitude normalized drag force versus slip at different frequency and magnetic parameters with separation $\lambda = 0.3$.

Therefore, Fig. 3 displays that the magnitude of drag force decreases with increases of the frequency for low or high values of frequency for various values of the separation parameter, $\lambda = 0.01, 0.25$ and decreases with the slip increases at constant magnetic parameter $\alpha = 0.01$. This figure shows that for a large distance between the sphere and the rigid wall the curves start from the same point at $|F/F_\infty| \rightarrow 1$ but for another value of the separation parameter at the starting point are dispersed. Moreover, in Fig.4 expositis for increases of the magnetic parameter, $\alpha = 0, 1.0, 4.0, 10.0$ the magnitude of drag force decreases at separation parameter, $\lambda = 0.3$.

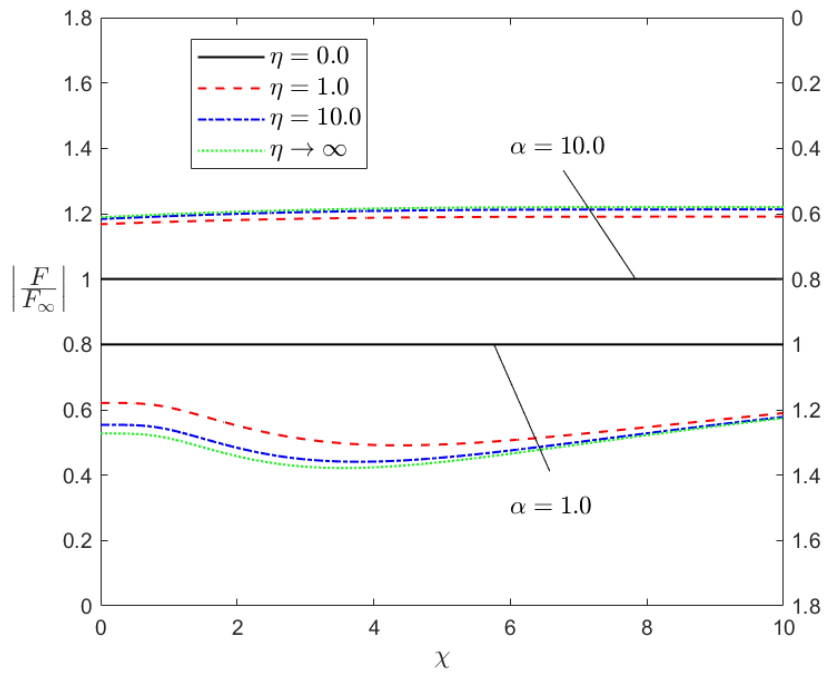


Figure 5: Magnitude normalized drag force versus frequency at different slip and magnetic parameters with separation $\lambda = 0.01$.

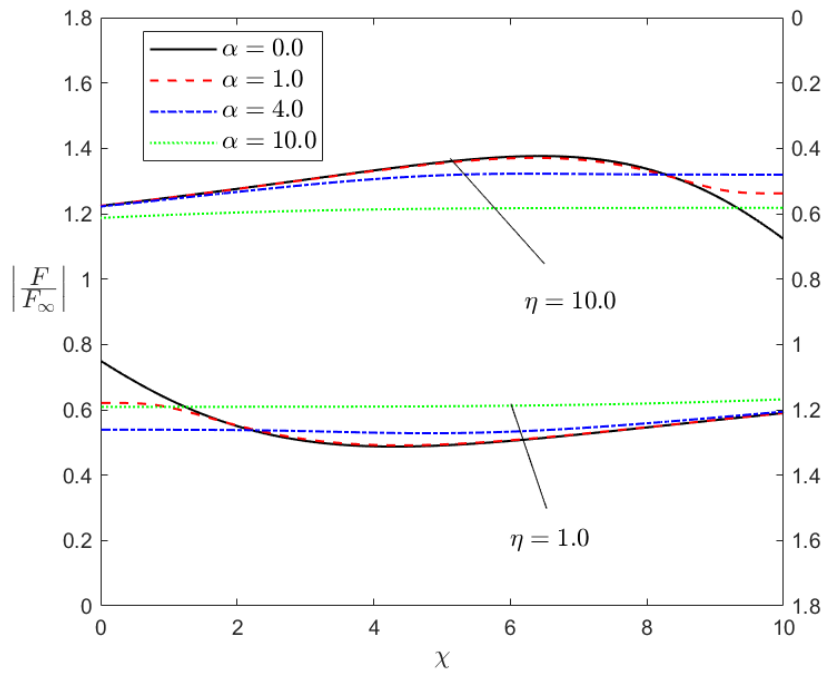


Figure 6: Magnitude normalized drag force versus frequency at different magnetic and slip parameters with separation $\lambda = 0.01$.

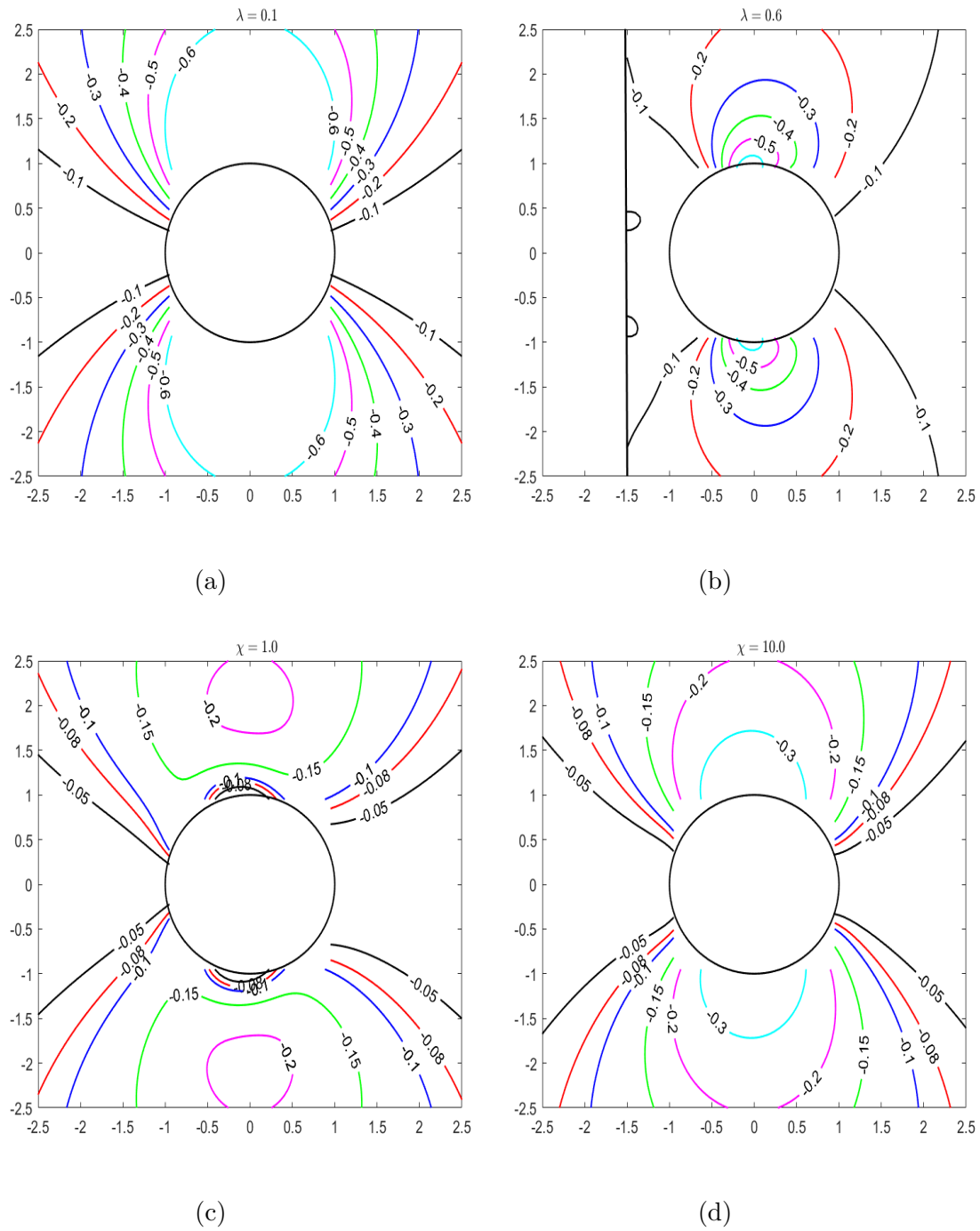


Figure 7: Streamlines distribution with various parameters

(a),(b) $\eta = 0.0, \chi = 10.0, \alpha = 4.0$ and (c),(d) $\eta = 10.0, \lambda = 0.25, \alpha = 1.0$.

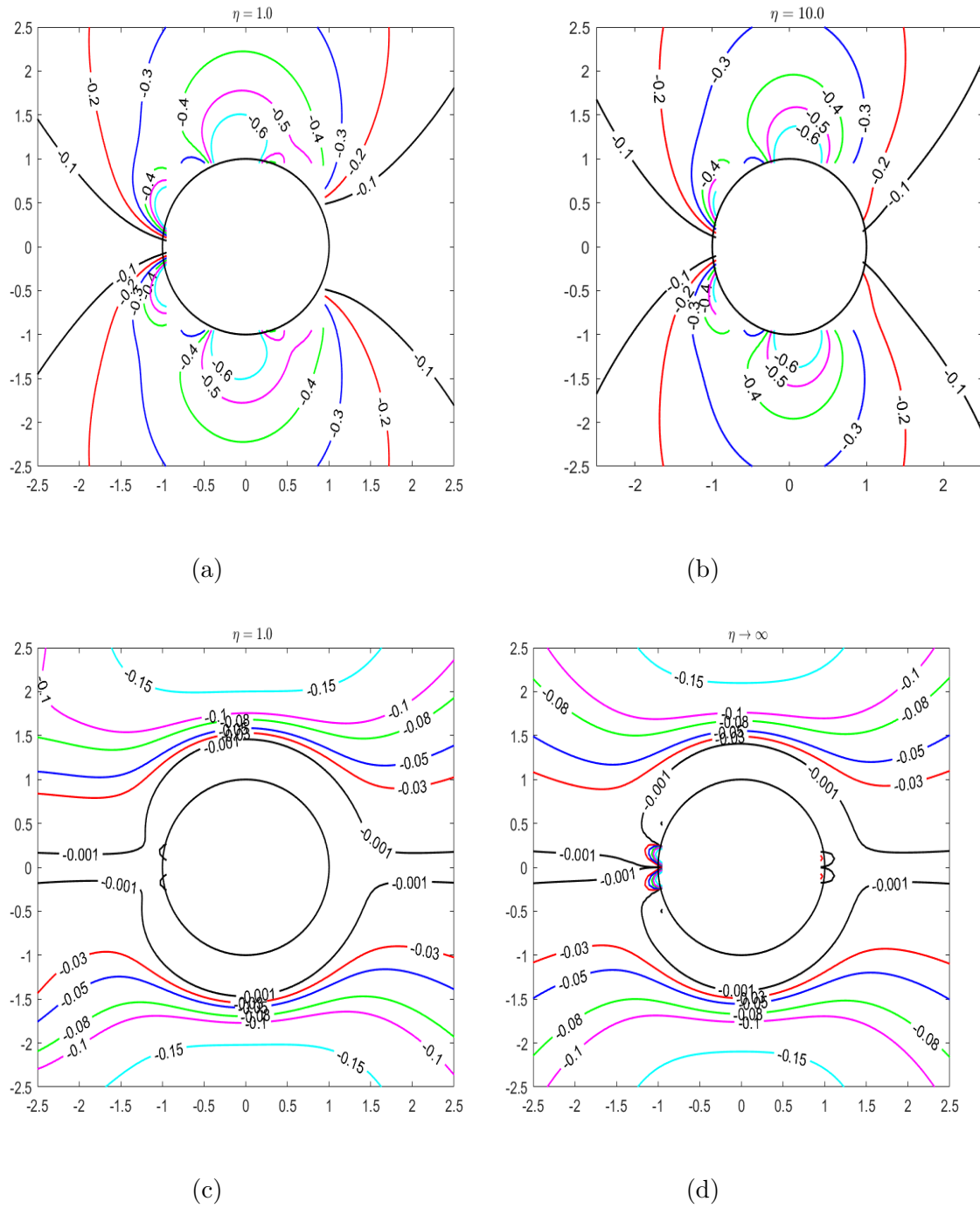
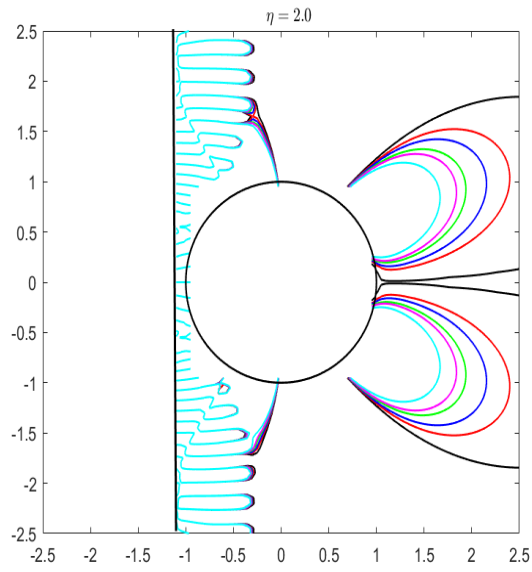
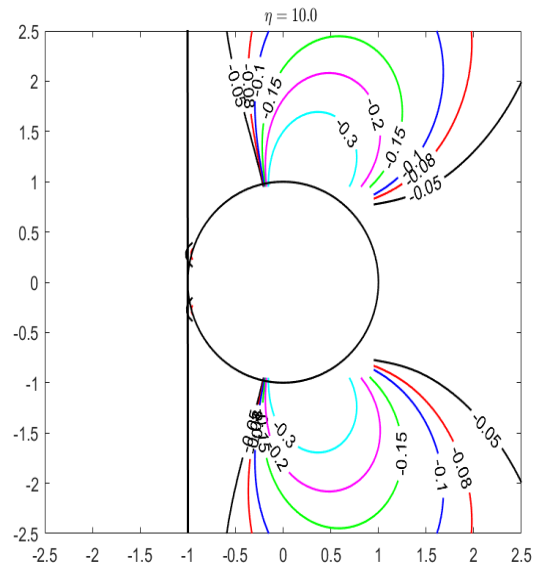


Figure 8: Streamlines distribution with various parameters

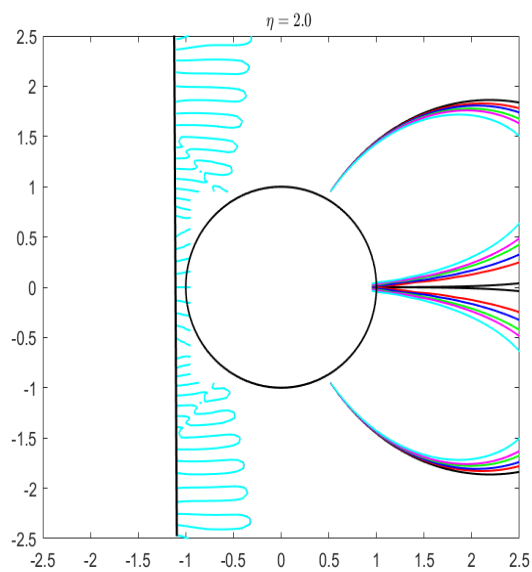
(a),(b) $\lambda = 0.25, \chi = 1.0, \alpha = 5.0$ and (c),(d) $\chi = 1.0, \lambda = 0.1, \alpha = 1.0$.



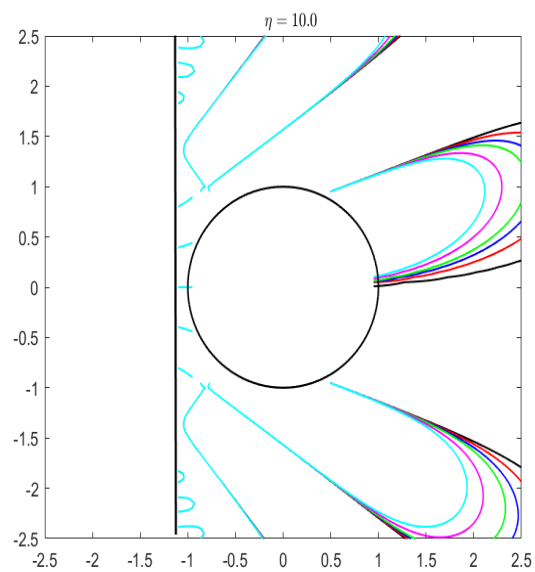
(a)



(b)



(c)



(d)

Figure 9: Streamlines distribution with various parameters

(a),(b) $\lambda = 0.9, \chi = 1.0, \alpha = 10.0$ and (c),(d) $\lambda = 0.9, \chi = 1.0, \alpha = 1.0$.

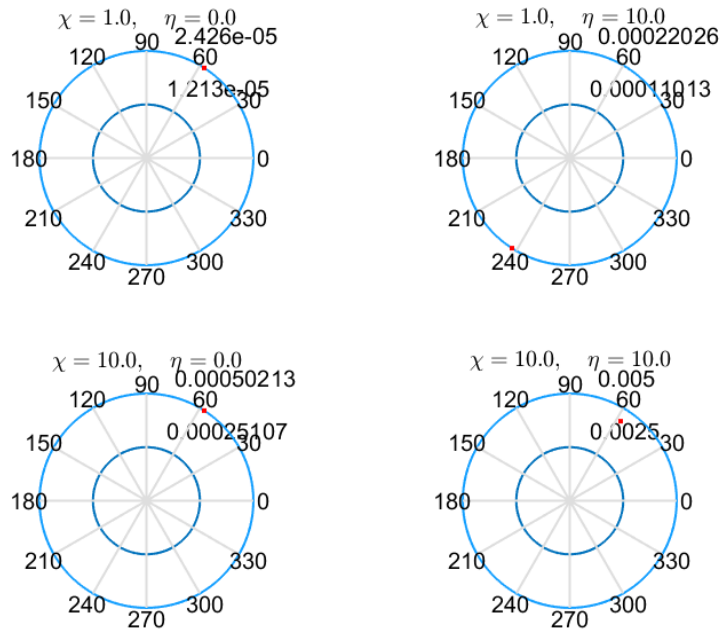


Figure 10: Phase angle for various parameters of the frequency and slip.

Furthermore, Fig. 5 shows that for increases of the slip for values, $\eta = 0, 1, 4, 10$ the magnitude of drag force decreases at $\lambda = 0.01$. It is obvious that for no slip it gives the limiting case, $|F/F_\infty| \rightarrow 1$ as known in the literature. Moreover, Fig.6 exhibits that the magnitude of drag force decreases with increases of the slip it raises for a high level at zero magnetic fields which is represented by the solid line and then intersected with the other curves at the point $(1.8, 0.48)$ for low frequency and again decay for high frequency for increasing of values of the magnetic parameter at $\lambda = 0.01$.

Steady streaming flows due to the motion of an oscillating sphere in a magnetic viscous fluid are responsible for a wide range of fluid phenomena. On the other side, Fig. 7-9 gives the streamlines for the stream function which can fully describe the variations of the flow pattern for different values of slip, magnetic, separation, and frequency parameters. Also, the figures describe the detailed structure of the streamline pattern. Eventually, the comparison shows an excellent agreement with the previous work of [41]. Accordingly, the streamlines of the flow around the oscillating sphere are very closed to the sphere and translate separately as one sphere at $\lambda = 0.1$. The interaction appears at the oscillating sphere near the rigid wall at $\lambda = 0.6$. The streamlines start from no-slip, $\eta = 0.0$ close to the sphere, and gradually close at the partial slip, $\eta = 1.0, 10.0$ to reach finally very closed at the perfect slip, $\eta \rightarrow \infty$. Fig. 10 represent the phase angle for various parameters of the frequency and slip.

Table 1: Magnitude normalized drag force versus at different slip, magnetic, separation and frequency parameters.

α	η	$\chi = 1.0$			$\chi = 4.0$		
		$\lambda = 0.001$	$\lambda = 0.1$	$\lambda = 0.25$	$\lambda = 0.001$	$\lambda = 0.1$	$\lambda = 0.25$
0.0	0.0	1.00000	0.99954	0.97001	1.00000	1.00010	1.00061
	2.0	0.58794	0.58769	0.57173	0.45466	0.45469	0.45394
	4.0	0.56184	0.56160	0.54642	0.43682	0.43684	0.43607
	6.0	0.55240	0.55217	0.53726	0.43072	0.43075	0.42997
	8.0	0.54753	0.54730	0.53253	0.42765	0.42768	0.42690
	10.0	0.54456	0.54433	0.52965	0.42580	0.42582	0.42504
2.0	0.0	1.00000	0.99914	0.96376	1.00000	0.99993	0.99258
	2.0	0.52345	0.52306	0.50699	0.47133	0.47127	0.46649
	4.0	0.50084	0.50047	0.48515	0.45401	0.45395	0.44924
	6.0	0.49283	0.49246	0.47739	0.44806	0.44800	0.44332
	8.0	0.48872	0.48836	0.47342	0.44505	0.44499	0.44032
	10.0	0.48623	0.48586	0.47101	0.44324	0.44318	0.43851
10.0	0.0	1.00000	0.99588	0.88678	1.00000	0.99753	0.91583
	2.0	0.51749	0.51548	0.45703	0.51707	0.51574	0.47014
	4.0	0.50287	0.50092	0.44384	0.50352	0.50222	0.45750
	6.0	0.49780	0.49586	0.43926	0.49885	0.49756	0.45313
	8.0	0.49523	0.49330	0.43693	0.49649	0.49520	0.45092
	10.0	0.49367	0.49175	0.43552	0.49506	0.49377	0.44958

6. Conclusion

The main physical theme has been the remarkable way in which the boundary conditions extend to include the slip influence with the existence of the magnetic fields and their effects on the magnitude of the normalized drag force and streamlines and their impacts are shows their practical significance in engineering and chemical reactions. Thus, oscillating spheres in the magnetic field have many applications for chemical reactions and nanoparticles interactions to generate heat through various mechanisms. In this study, we have presented a combined analytical and numerical solution procedure for the Stokes flow caused by an oscillating sphere embedded in a magnetic viscous fluid with slip. The sphere oscillates along an axis normal to an unbounded rigid wall. Boundary conditions are satisfied first at the plane wall by the Fourier–Bessel transform and then on the sphere surface by a collocation technique. The numerical results of the magnitude of drag force acting on the sphere by the external fluid show that the solution procedure converges rapidly. For various values of the clearance (separation parameter), the slip, magnetic parameter, and frequency parameter comparisons with the limiting cases available in the literature. Besides engineering applications - the present analysis of the magnetic oscillating sphere towards the plate problem possesses also geophysical and astrophysical applications; namely, in connection with the use of such equations for a better understanding of the motion of

electrically conducting fluids - such as [47].

References

- [1] K R Cramer and S I Pai. Magnetofluid dynamics for engineers and applied physicists. *McGraw-Hill Book Company*, page 347, 1973.
- [2] A Sellier and S Aydin. Maxisymmetric mhd viscous flows bounded by a solid plane normal to a uniform ambient magnetic field: fundamental flows and application to a solid sphere translating normal to the wall. *European Journal of Computational Mechanics*, 27:443–468, 2018.
- [3] N F Okechi and S Asghar. Mhd stokes flow in a corrugated curved channel, chinese journal of physics. *Chinese Journal of Physics*, 71:38–53, 2021.
- [4] S Qian and H H Bau. Magneto-hydrodynamic stirrer for stationary and moving fluids. *Sensors and Actuators B: Chemical*, 106:859–870, 2005.
- [5] S El-Sapa and N S Alsudais. Effect of magnetic field on the motion of two rigid spheres embedded in porous media with slip surfaces. *The European Physical Journal E*, 44:1–11, 2021.
- [6] R Chaudhary and A Jain. Combined heat and mass transfer effects on mhd free convection flow past an oscillating plate embedded in porous medium. *Romanian Journal of Physics*, 52:505–524, 2007.
- [7] J Raza, F Mebarek-Oudina, and A J Chamkha. Magnetohydrodynamic flow of molybdenum disulfide nanofluid in a channel with shape effects. *Multidiscipline Modeling in Materials and Structures*, 2017.
- [8] H S Takhar and G Nath A J Chamkha. Mhd flow over a moving plate in a rotating fluid with magnetic field, hall currents and free stream velocity, international journal of engineering science. *International Journal of Engineering Science*, 40:1511–1527, 2002.
- [9] M V Krishna, N A Ahamad, and A J Chamkha. Hall and ion slip effects on unsteady mhd free convective rotating flow through a saturated porous medium over an exponential accelerated plate. *Alexandria Engineering Journal*, 59:565–577, 2020.
- [10] M V Krishna and A J Chamkha. Hall and ion slip effects on mhd rotating flow of elastico-viscous fluid through porous medium, international communications in heat and mass transfer. *International Communications in Heat and Mass Transfer*, 113:104494, 2020.
- [11] I Chabani, F Mebarek-Oudina, and A A I Ismail. Mhd flow of a hybrid nano-fluid in a triangular enclosure with zigzags and an elliptic obstacle, micromachines. *Micromachines*, 13:224, 2022.

- [12] R Djebali, F Mebarek-Oudina, and C Rajashekhar. Similarity solution analysis of dynamic and thermal boundary layers: further formulation along a vertical flat plate. *Physica Scripta*, 96:085206, 2021.
- [13] S Marzougui, F Mebarek-Oudina, M Magherbi, and A McHirgui. Entropy generation and heat transport of cu–water nanoliquid in porous lid-driven cavity through magnetic field. *International Journal of Numerical Methods for Heat Fluid Flow*, 32:2047–2069, 2021.
- [14] Y D Reddy, F Mebarek-Oudina, B S Goud, and A I Ismail. Velocity and thermal slips effect toward mhd boundary layer flow through heat and mass transport of williamson nanofluid with porous medium. *Arabian Journal for Science and Engineering*, 2022.
- [15] A S Warke, K Ramesh, F Mebarek-Oudina, and A Abidi. Numerical investigation of the stagnation point flow of radiative magnetomicropolar liquid past a heated porous stretching sheet. *Journal of Thermal Analysis and Calorimetry*, 147:6901–6912, 2022.
- [16] C Y Wang. The flow field induced by an oscillating sphere. *Journal of Sound and Vibration*, 2:257–269, 1965.
- [17] T Rikitake. Magneto-hydrodynamic oscillations of a perfectly conducting fluid sphere placed in a uniform magnetic field. *Journal of the Physical Society of Japan*, 12:1224–1230, 1958.
- [18] S Chawla. Magnetohydrodynamic oscillatory flow past a semi-infinite flat plate. *International Journal of Non-Linear Mechanics*, 6:117–134, 1971.
- [19] W Zhang, J Peng, and S Li. Damping force modeling and suppression of self-excited vibration due to magnetic fluids applied in the torque motor of a hydraulic servovalve. *Energies*, 10:749, 2017.
- [20] T Rikitake. Immersed boundary and overset grid methods assessed for stokes flow due to an oscillating sphere. *Journal of Computational Physics*, 423:109783, 2020.
- [21] R Mei, J Xiong, and R Tran-Son-Tay. Motion of a sphere oscillating at low reynolds numbers in a viscoelastic-fluid-filled cylindrical tube. *Journal of Non-Newtonian Fluid Mechanics*, 66:169–192, 1996.
- [22] P Trevizoli, Y Liu, A Tura, A Rowe, and J Barbosa. Experimental assessment of the thermal–hydraulic performance of packed-sphere oscillating-flow regenerators using water. *Experimental Thermal and Fluid Science*, 57:324–334, 2014.
- [23] R S Alassar and H M Badr. Oscillating viscous flow over a sphere. *Computers Fluids*, 26:661–682, 1997.
- [24] V Polunin, P Ryapolov, A Zhakin, E Shel’deshova, and G Karpova. “wall viscosity” of magnetic fluid oscillations in a strong magnetic field. *Russian Physics Journal*, 62:589–597, 2019.

- [25] P Ryapolov, V Polunin, G Alisher, and E Shel'deshova. The influence of the viscosity on the oscillations of the element of magnetic fluid in the magnetic field. *in: EPJ Web of Conferences, EDP Sciences*, page 00061, 2019.
- [26] O Ustundag, N Bakir, A Gumenyuk, and M Rethmeier. Influence of oscillating magnetic field on the keyhole stability in deep penetration laser beam welding. *Optics Laser Technology*, 135:106715, 2021.
- [27] M S Faltas and S El-Sapa. Rectilinear oscillations of two spherical particles embedded in an unbounded viscous fluid. *Microsystem Technologies*, 25:39–49, 2019.
- [28] H Sherief, M Faltas, and S El-Sapa. Force on a spherical particle oscillating in a viscous fluid perpendicular to an impermeable plane wall. *Journal of the Brazilian Society of Mechanical Sciences and Engineering*, 41:1–10, 2019.
- [29] E A Ashmawy. Rotary oscillation of a composite sphere in a concentric spherical cavity using slip and stress jump conditions. *The European Physical Journal Plus*, 130:163, 2015.
- [30] C A Sweeney, W Vorster, S B Leen, E Sakurada, P E McHugh, and F P E Dunne. The role of elastic anisotropy, length scale and crystallographic slip in fatigue crack nucleation. *Journal of the Mechanics and Physics of Solids*, 61:1224–1240, 2013.
- [31] L Basnayaka, B Albijanic, N Subasinghe, and R Panjipour. Influence of slip length on filtration performance of fine particles. *Powder Technology*, 32:1333–1340, 2021.
- [32] C Sulochana, S P Samrat, and N Sandeep. Numerical investigation of magnetohydrodynamic (mhd) radiative flow over a rotating cone in the presence of solet and chemical reaction advanced. *Propulsion and Power Research*, 7:91–101, 2018.
- [33] M Veera Krishna, N A Ahamad, and A J Chamkha. Numerical investigation on unsteady mhd convective rotating flow past an infinite vertical moving porous surface. *Ain Shams Engineering Journal*, 12:2099–2109, 2021.
- [34] E A Ashmawy. Wall effects on a rigid sphere moving perpendicular to a plane wall in a couple stress fluid filling a half-space. *European Journal of Mechanics - B/Fluids*, 74:380–388, 2019.
- [35] S El-Sapa, E I Saad, and M S Faltas. Axisymmetric motion of two spherical particles in a brinkman medium with slip surfaces. *European Journal of Mechanics - B/Fluids*, 67:306–313, 2018.
- [36] H H Sherief, M S Faltas, and S El-Sapa. Axisymmetric creeping motion caused by a spherical particle in a micropolar fluid within a nonconcentric spherical cavity. *European Journal of Mechanics - B/Fluids*, 77:211–220, 2019.

- [37] H H Sherief, M S Faltas, and S El-Sapa. Interaction between two rigid spheres moving in a micropolar fluid with slip surfaces. *Journal of Molecular Liquids*, 290:111165, 2019.
- [38] S El-Sapa. Interaction between a non-concentric rigid sphere immersed in a micropolar fluid and a spherical envelope with slip regime. *Journal of Molecular Liquids*, 351:118611, 2022.
- [39] S El-Sapa and M S Faltas. Mobilities of two spherical particles immersed in a magnetomicropolar fluid. *Physics of Fluids*, 34:013104, 2022.
- [40] P K Yadav, S Deo, S P Singh, and A Filippov. Effect of magnetic field on the hydrodynamic permeability of a membrane built up by porous spherical particles. *Colloid Journal*, 79:160–171, 2017.
- [41] J Happel and H Brenner. Low reynolds number flow hydrodynamics. *Martinus Nijhoff publishers, The Hague*, 1983.
- [42] Willers, A. Erdélyi, W. Magnus, F. Oberhettinger, and F. G. Tricomi. Tables of integral transforms. *Vol. I. (Based, in part, on notes left by Harry Batemann, Late Prof. at the California. Institute of Technology). XX + 391 S. New York/Toronto/London 1954. McGraw-Hill Book Comp., Inc. Preis 56/6 s, ZAMM - Journal of Applied Mathematics and Mechanics / Zeitschrift für Angewandte Mathematik und Mechanik*, 34:478–478, 1954.
- [43] R S Chadwick and Z Liao. High-frequency oscillations of a sphere in a viscous fluid near a rigid plane. *SIAM review*, 50:313–322, 2008.
- [44] H S Sellers, W H Schwarz, M Sato, and T Pollard. Boundary effects on the drag of an oscillating sphere: applications to the magnetic sphere rheometer. *Journal of Non-Newtonian Fluid Mechanics*, 26:43–55, 1987.
- [45] C J Lawrence and S Weinbaum. The force on an axisymmetric body in linearized, time-dependent motion: a new memory term. *Journal of Fluid Mechanics*, 171:209–218, 1986.
- [46] L E Payne and W H Pell. The stokes flow problem for a class of axially symmetric bodies. *Journal of Fluid Mechanics*, 7:529–549, 1960.
- [47] V J Rossow. Nasa tech. *Note 3971*, 1957.

Appendix

The functions appearing in equation, (30)-(31) and (38)-(39) are defined as:

$$\begin{aligned}
 A_{1n}(r, \theta) &= -r^{(-n-1)}(n+1)\mathfrak{S}_{n+1}(\cos \theta) \csc \theta. \\
 B_{1n}(r, \theta) &= -r^{\frac{-3}{2}} \left(krK_{n-\frac{3}{2}}(kr) \cos \theta \mathfrak{S}_n(\cos \theta) + (n+1)K_{n-\frac{1}{2}}(kr)\mathfrak{S}_{n+1}(\cos \theta) \right) \csc \theta. \\
 A_{2n}(r, \theta) &= -r^{(-n-1)}P_n(\cos \theta) \\
 B_{2n}(r, \theta) &= r^{\frac{-3}{2}} \left(krK_{n-\frac{3}{2}}(kr)\mathfrak{S}_n(\cos \theta) - K_{n-\frac{1}{2}}(kr)P_n(\cos \theta) \right) \csc \theta. \\
 A_{3n}(r, \theta) &= 2(n^2 - 1)r^{-n-2}\mathfrak{S}_n(\cos \theta) \csc \theta \\
 B_{3n}(r, \theta) &= r^{-\frac{5}{2}} \left((k^2r^2 + 2n(n-2))K_{n-\frac{1}{2}}(kr) + 2krK_{n+\frac{1}{2}}(kr) \right) \mathfrak{S}_{n+1}(\cos \theta) \csc \theta \\
 L(\tau, -b) &= (\tau - \xi)^{-1} \sum_{n=2}^{\infty} \left[(\tau e^{-\sigma} - \xi e^{-\delta})e_{1n}(\tau, -b) + \xi(-e^{-\sigma} + e^{-\delta})e_{2n}(\tau, -b) \right] A_n \\
 &+ \left[(\tau e^{-\sigma} - \xi e^{-\delta})f_{1n}(\tau, -b) + \xi(-e^{-\sigma} + e^{-\delta})f_{2n}(\tau, -b) \right] B_n \\
 M(\tau, -b) &= (\tau - \xi)^{-1} \sum_{n=2}^{\infty} \left[\tau(e^{-\sigma} - e^{-\delta})e_{1n}(\tau, -b) + (-e^{-\sigma} + \tau e^{-\delta})e_{2n}(\tau, -b) \right] A_n \\
 &+ \left[\tau(e^{-\sigma} - e^{-\delta})f_{1n}(\tau, -b) + \xi(-\xi e^{-\sigma} + \tau e^{-\delta})f_{2n}(\tau, -b) \right] B_n \\
 R_{(r,\theta)} &= r^{-2} \left(2A(\tau) \left[r \cos \theta + r^2 \cos 2\theta \right] e^{-\tau z} + B(\tau)\tau^{-1} \left[2\xi r \cos \theta + r^2 \cos 2\theta(\tau^2 + \xi^2) \right] e^{-\xi z} \right) \\
 S(r, \theta) &= -4 \cos^2 \theta (\tau A(\tau) e^{-\tau z} + \xi B(\tau) e^{-\xi z}) \\
 e_{1n}(\tau, -b) &= (-1)^{n-1} \frac{\tau^{n-1}}{n!} e^{-b\tau} \\
 e_{2n}(\tau, -b) &= (-1)^n \frac{\tau^{n-1}}{n!} e^{-b\tau} \\
 f_{1n}(\tau, -b) &= (-1)^n \sqrt{\frac{\pi k}{2\tau^2}} e^{-b\xi} \mathfrak{S}_n\left(\frac{\xi}{k}\right) \\
 f_{2n}(\tau, -b) &= (-1)^{n-1} \sqrt{\frac{\pi k}{2\xi^2}} e^{-b\xi} \mathfrak{S}_n\left(\frac{\xi}{k}\right) \\
 \gamma_{1n}^{(1)} &= A_{1n}(1, \theta) + a_{1n}^{(1)}, \quad \gamma_{2n}^{(1)} = B_{1n}(1, \theta) + b_{1n}^{(1)}, \\
 \gamma_{1n}^{(2)} &= A_{2n}(1, \theta) + a_{2n}^{(1)}, \quad \gamma_{2n}^{(1)} = B_{2n}(1, \theta) + b_{2n}^{(1)}, \\
 \gamma_{1n}^{(*)} &= A_{3n}(1, \theta) + a_{1n}^{(*)}, \quad \gamma_{2n}^{(*)} = B_{3n}(1, \theta) + b_{1n}^{(*)}, \\
 \begin{pmatrix} a_{1n}^{(1)}(r, \theta) \\ b_{1n}^{(1)}(r, \theta) \end{pmatrix} &= \int_0^\infty \tau \left\{ H_1 \begin{pmatrix} e_{1n}(\tau, -b) \\ f_{1n}(\tau, -b) \end{pmatrix} + H_2 \begin{pmatrix} e_{2n}(\tau, -b) \\ f_{2n}(\tau, -b) \end{pmatrix} \right\} J_1(r \sin \theta \tau) d\tau \\
 \begin{pmatrix} a_{2n}^{(1)}(r, \theta) \\ b_{2n}^{(1)}(r, \theta) \end{pmatrix} &= \int_0^\infty \tau \left\{ H_3 \begin{pmatrix} e_{1n}(\tau, -b) \\ f_{1n}(\tau, -b) \end{pmatrix} + H_4 \begin{pmatrix} e_{2n}(\tau, -b) \\ f_{2n}(\tau, -b) \end{pmatrix} \right\} J_1(r \sin \theta \tau) d\tau
 \end{aligned}$$

$$\begin{aligned}
& \begin{pmatrix} a_{1n}^{(*)}(r, \theta) \\ b_{1n}^{(*)}(r, \theta) \end{pmatrix} \\
= & \int_0^\infty \tau \left\{ H_5 \begin{pmatrix} e_{1n}(\tau, -b) \\ f_{1n}(\tau, -b) \end{pmatrix} + H_6 \begin{pmatrix} e_{2n}(\tau, -b) \\ f_{2n}(\tau, -b) \end{pmatrix} \right\} J_1(r \sin \theta \tau) d\tau \\
+ & \int_0^\infty \tau \left\{ H_7 \begin{pmatrix} e_{1n}(\tau, -b) \\ f_{1n}(\tau, -b) \end{pmatrix} + H_8 \begin{pmatrix} e_{2n}(\tau, -b) \\ f_{2n}(\tau, -b) \end{pmatrix} \right\} J_0(r \sin \theta \tau) d\tau \\
H_1 = & (\tau - \xi)^{-1} (\tau e^{-\sigma} - \xi e^{-\delta}) \\
H_2 = & \xi (\tau - \xi)^{-1} (-e^{-\sigma} + e^{-\delta}) \\
H_3 = & \tau (\tau - \xi)^{-1} (e^{-\sigma} - e^{-\delta}) \\
H_4 = & (\tau - \xi)^{-1} (-\xi e^{-\sigma} + \tau e^{-\delta}) \\
H_5 = & (\rho^2 + z^2)^{-1} (\tau - \xi)^{-1} [-2\tau(z + (z^2 - \rho^2)) e^{-\sigma} + (2z\xi + (z^2 - \rho^2)(\tau^2 + \xi^2)) e^{-\delta}] \\
H_6 = & \tau(\rho^2 + z^2)^{-1} (\tau - \xi)^{-1} [2\xi(z + (z^2 - \rho^2)) e^{-\sigma} - (2z\xi + (z^2 - \rho^2)(\tau^2 + \xi^2)) e^{-\delta}] \\
H_7 = & -4z(\rho^2 + z^2)^{-1} (\tau - \xi)^{-1} (-\tau^2 e^{-\sigma} + \xi\tau e^{-\delta}) \\
H_8 = & -4z\xi\tau(\rho^2 + z^2)^{-1} (\tau - \xi)^{-1} (e^{-\sigma} - e^{-\delta}) \\
\sigma = & \tau(b + r \cos \theta), \quad \delta = \xi(b + r \cos \theta)
\end{aligned}$$